Di Li[1]
Jessica Zielinski[2]
Lukasz Kozubowski[2]
Xiangchun Xuan[1]

[1]Department of Mechanical Engineering, Clemson University, Clemson, SC, USA
[2]Department of Genetics and Biochemistry, Clemson University, Clemson, SC, USA

Received November 13, 2017
Revised February 13, 2018
Accepted February 14, 2018

Research Article

Continuous sheath-free separation of drug-treated human fungal pathogen *Cryptococcus neoformans* by morphology in biocompatible polymer solutions

Cryptococcal meningitis caused by *Cryptococcus neoformans* is the leading cause of fungal central nervous system infections. Current antifungal treatments for cryptococcal infections are inadequate partly due to the occurrence of drug resistance. Recent studies indicate that the treatment of the azole drug fluconazole changes the morphology of *C. neoformans* to form enlarged "multimeras" that consist of three or more connected cells/buds. To analyze if these multimeric cells are a prerequisite for *C. neoformans* to acquire drug resistance, a tool capable of separating them from normal cells is critical. We extend our recently demonstrated sheath-free elasto-inertial particle separation technique to fractionate drug-treated *C. neoformans* cells by morphology in biocompatible polymer solutions. The separation performance is evaluated for both multimeric and normal cells in terms of three dimensionless metrics: efficiency, purity, and enrichment ratio. The effects of flow rate, polymer concentration, and microchannel height on cell separation are studied.

Keywords:
Cell separation / Elasticity / Inertia / Microfluidics / Morphology
DOI 10.1002/elps.201700428

1 Introduction

Cryptococcal meningitis caused by *Cryptococcus neoformans* (an encapsulated yeast) is the leading cause of fungal central nervous system infections in the world, primarily in immune-compromised patients [1]. Despite mounting public health threats, current treatments for cryptococcal infections are still inadequate. This is partly because *C. neoformans* acquires resistance to fluconazole, an azole antifungal drug, by becoming aneuploid with an increased copy number of key resistance genes [2]. Recent studies indicate that fluconazole treatment changes the morphology of *C. neoformans* from either round, unbudded cells, or cells with a single bud, to enlarged "multimeras" that consist of at least three cells connected together (Figure 1) [3]. To analyze if the formation of multimeric cells is a prerequisite for *C. neoformans* to acquire drug resistance, a tool capable of separating them from normal cells is critical.

Microfluidic devices have been extensively used to separate and sort cells due to a number of advantages over their macro-scale counterparts such as enhanced efficiency, improved accuracy, and reduced cost etc. [4, 5]. Cell separation based on intrinsic properties (e.g., size and density) in a continuous flow has become a recently increasing trend [6]. However, the majority of these label-free microfluidic approaches are restricted to separating cells with dissimilar sizes, which often becomes inefficient at handling real samples due to the inherent deviation in cell size [7]. It is thus desirable to combine two or more intrinsic cell properties to develop a multiparameter cell separation technique for practical biomedical applications. A potential passive biomarker could be morphology, which incorporates multiple aspects of cells including size, shape, and structure. It is a fundamental cell property [8] that provides important information on cell synchronization [9], disease diagnostic [10], etc. Only recently has the morphology (or simply shape) been utilized to separate particles or cells in microfluidic devices. These microfluidic separations can take place in either a batchwise or a continuous manner, where the best example of the former is CE [11].

The continuous-flow separations can be classified into two categories: one uses a sheath flow to pre-focus particles or cells prior to separation in the transverse direction (termed sheath-focusing separation), and the other uses a force field to direct particles or cells toward morphology-dependent equilibrium positons in the flow (termed sheath-free separation). The first sheath-focusing separation of particles by morphology was reported by Sugaya et al. [12], who extended their

Correspondence: Professor Xiangchun Xuan, Department of Mechanical Engineering, Clemson University, Clemson, SC 29634-0921, USA
Fax: +1-864-656-7299
E-mail: xcxuan@clemson.edu

Abbreviations: ***C. neoformans***, Cryptococcus neoformans; **FCF**, forcholorfenuron; **PEO**, polyethylene oxide; **YPD**, extract peptone dextrose

Color Online: See the article online to view Figs. 1–7 in color.

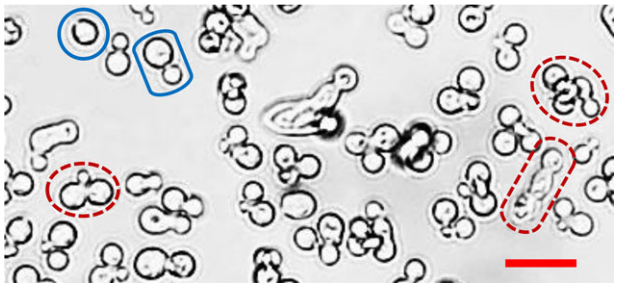

Figure 1. Close-up view of drug-treated *C. neoformans* cells, which are divided into two primary groups based on morphology: one is normal cells with no buds or single buds (highlighted using the solid-line boxes), and the other is multimeric cells that consist of at least three connected cells/buds (highlighted using the dashed-line boxes). The scale bar represents 10 μm.

developed hydrodynamic filtration technique [13] to separate pre-aligned spherical and non-spherical polystyrene particles in a network of microchannels. Beech et al. [14] utilized the deterministic lateral displacement [15] to place morphologically altered red blood cells to dissimilar streamlines in a laminar flow around an array of obstacles. Recently, Lu and Xuan [16] demonstrated an efficient separation of equal-volumed spherical and peanut-shaped polystyrene particles in a viscoelastic polyethylene oxide (PEO) solution via elasto-inertial pinched flow fractionation [17]. Zhou and Xuan [18] used the shape-dependent magnetophoretic motion to separate a sheath-focused mixture of spherical and non-spherical particles in a ferrofluid. This magnetic method was later extended by the same group to fractionate a heterogeneous mixture of yeast cells by morphology [19]. More recently, Zhou et al. [20] separated prefocused magnetic particles of dissimilar shapes under a uniform magnetic field via the shape-dependent magnetic rotation [21].

Compared to sheath-focusing particle and cell separations, sheath-free separations eliminate the sheath flow that is usually driven at a much higher flow rate than the particle/cell suspension itself. Therefore, the flow control in sheath-free separations is much simpler and the concentration of the separated particles/cells therein is much less diluted [4–7]. Among sheath-free particle and cell separations by morphology, Valero et al. [22] employed multi-frequency dielectrophoresis [23] to synchronize the yeast cell division. Kose et al. [24] exploited the morphology-dependent AC field-driven magnetic force and torque to separate sickle and healthy red blood cells in a ferrofluid. DuBose et al. [25] demonstrated a low-throughput DC field-driven separation of spherical and non-spherical particles in a spiral microchannel via curvature-induced dielectrophoresis [26]. In contrast, Masaeli et al. [27] achieved a high-throughput inertial sorting of spheroid particles with different aspect ratios as well as yeast cells at different cell cycle stages in a straight rectangular microchannel. A similar method was later used by the same group to separate microalga *Euglena gracilis* [28]. Recently, Lu et al. [29] demonstrated a sheathless separation of equal-volumed spherical and peanut-shaped polystyrene particles in the flow of a viscoelastic polymer solution. The intermediate flow throughput of this elasto-inertial separation fills the gap between the dielectrophoretic [25] and inertial separations [27] with a high efficiency and purity.

We extend in this work our recently demonstrated sheath-free elasto-inertial separation of polystyrene particles [29, 30] to fractionate drug-treated *C. neoformans* cells by morphology. The variations in cell shape and size, induced by drug treatment, are incompatible with the majority of existing cell separation methods because the force experienced by a cell in nearly every field decreases for less spherical cells while increases for larger cells. Therefore, the transverse motion of larger irregular-shaped yeast cells becomes similar to that of smaller round-shaped ones under the application of a single force field. Our elasto-inertial particle separation technique [29, 30] resolves this issue by the use of the competing components of flow-induced elastic and inertial lift forces in biocompatible polymer solutions. We will perform a systematic experimental study of the factors that affect the cell separation performance.

2 Materials and methods

2.1 Preparation and drug-treatment of yeast cells

C. neoformans strain H99 cells [31] were grown overnight at 24°C in the yeast extract peptone dextrose (YPD) medium. They were refreshed next day to a density of 10^7 cells/mL before the treatment of forchlorfenuron (FCF) (CAS Number: 61857-60-8, Sigma–Aldrich), a synthetic plant cytokinin that has been reported to interrupt cytokinesis in *Saccharomyces cerevisiae* [32]. The culture of *C. neoformans* was incubated in the YPD medium with 0.25 mM FCF overnight at 37°C. The treated cells were then fixed with 3.7% formaldehyde for 1 h and spun down followed by the re-suspension in the PBS solution for later experiments. Figure 1 shows a zoom-in image of the FCF-treated yeast cells that exhibit aberrant morphology. We divided these cells into two primary groups for analysis: one group with regular morphologies was the normal cells that have no buds or single bugs, and the other group with abnormal morphologies was the multimeric cells that have three or more connected cells/buds. The equivalent spherical diameter of each group of yeast cells was determined using the geometry package in COMSOL® via a three-dimensional model with the measured cell dimensions and structure (assuming spherical for each cell or bud). The average equivalent spherical diameter is approximately 5 and 7 μm for the normal and multimeric cells, respectively, as demonstrated in our recent experimental and numerical study of cell magnetophoresis in dilute ferrofluids [19].

2.2 Manipulation of drug-treated yeast cells in polymer solutions

Prior to experiment, the FCF-treated *C. neoformans* cells were re-suspended in PBS-based PEO solutions at a density of

Table 1. Rheology properties (at 20°C) of the prepared PBS-based PEO solutions [16, 30]

Properties	PEO concentration (ppm)		
	500	1000	2000
density (ρ, g/cm^3)	1.0	1.0	1.0
zero-shear viscosity (η_0, mPa·s)	1.8	2.3	4.1
effective relaxation time (λ, ms)	4.3	6.8	10.6

10^5–10^6 cells/ml. Three concentrations of PEO solutions, i.e., 500, 1000, and 2000 ppm, were made by dissolving PEO powder (molecular weight, $M_w = 2 \times 10^6$ Da, Sigma–Aldrich) into the PBS solution. The rheology properties of these polymer solutions are listed in Table 1 [16, 30]. The prepared yeast cell suspension was injected into a straight rectangular microchannel using a syringe pump (KD Scientific). Figure 2A shows a top-view picture of the channel, which was fabricated with PDMS using the standard soft lithography method. The channel is 50 μm wide and 2 cm long followed by a 900 μm wide and 2 mm long sudden expansion at the outlet for enhanced cell separation and visualization. Three channel heights, i.e., 15, 25, and 40 μm, were used in experiments. The translational motion of cells was visualized through an inverted microscope (Nikon Eclipse TE2000U, Nikon Instruments) with a CCD camera (Nikon DS-Qi1Mc) at a rate of around 15 frames/s. The rotational motion of cells was not tracked due to the limited speed of our imaging system, which will be left for a potential future study. The obtained digital images were processed using the Nikon imaging software (NIS-Elements), and further analyzed using the ImageJ software (National Institute of Health).

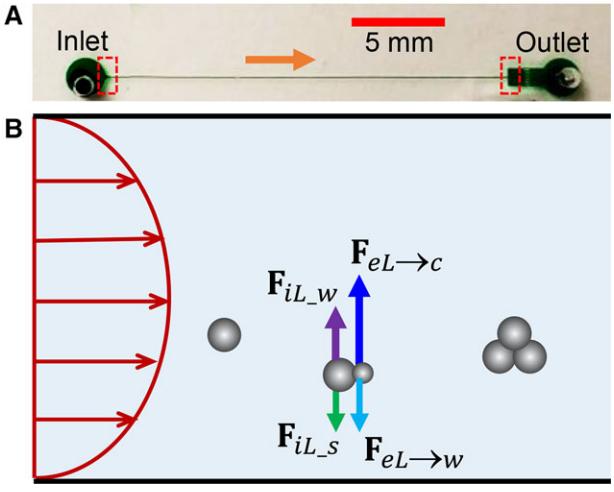

Figure 2. (A) Top-view picture of the straight rectangular microchannel used in experiments, where the block arrow indicates the flow direction and the dashed-line boxes highlight the windows of view at the channel inlet and outlet, respectively. (B) Force analysis on a suspended cell in the flow of viscoelastic polymer solutions through a straight rectangular microchannel (see the text for the definitions of symbols).

2.3 Test of yeast cell viability

In order to assess the polymer effects on cell viability, the untreated *C. neoformans* cell suspension was subjected to separation in PBS-based 1000 ppm PEO solution and counted. Approximately 10 000 yeast cells were then plated on a semisolid YPD medium. After 1 day of growth at room temperature, plates were examined under the microscope to assess the percentage of cells that grew into colonies. It was found that the survival rate of yeast cells in the polymer solution was close to 100%. This observation of biocompatibility is also supported by recently reported studies on the manipulation of several types of other cells (e.g., bacteria, blood cells, and cancer cells) in PEO solutions [33–36].

3 Theory

3.1 Mechanism of cell separation

Figure 2B shows the inherently induced lift forces on a suspended cell in the flow of viscoelastic fluids through a straight rectangular microchannel. The elastic lift is a result of the normal stress difference [37–39] over the channel cross-section. It has been suggested in recent studies [30, 40] to be viewed as a combination of two opposing force components: one is the center-directed elastic lift component, $\mathbf{F}_{eL\to c}$, due to fluid elasticity, and the other is the wall-directed elastic lift component, $\mathbf{F}_{eL\to w}$, due to fluid elasticity and shear thinning. The total elastic lift, $\mathbf{F}_{eL} = \mathbf{F}_{eL\to c} + \mathbf{F}_{eL\to w}$, is expressed in the following scale [41],

$$\mathbf{F}_{eL} \sim d^3 \lambda \nabla \dot{\gamma}^2, \tag{1}$$

where d is the (equivalent) spherical cell diameter, λ is the fluid relaxation time, and $\dot{\gamma}$ is the fluid shear rate. It increases with the Weissenberg number, Wi,

$$Wi = \lambda \dot{\gamma} = \lambda \frac{2U}{w} = \frac{2\lambda Q}{w^2 h} \tag{2}$$

where U is the average fluid velocity, w is the channel width, Q is the volumetric flow rate, and h is the channel height.

The wall-induced inertial lift component, $\mathbf{F}_{iL\_w}$, pushes a cell away from the channel wall. The shear gradient-induced inertial lift component, $\mathbf{F}_{iL\_s}$, directs the cell towards the wall [42]. The balance of these two inertial lift components yields equilibrium cell positions that are a weak function of cell size or shape in straight rectangular microchannels [43]. The total inertial lift, $\mathbf{F}_{iL} = \mathbf{F}_{iL\_w} + \mathbf{F}_{iL\_s}$, has been theoretically proved to scale as [44],

$$F_{iL} \sim \rho d^4 \dot{\gamma}^2 \tag{3}$$

where ρ is the fluid density. This force is a strong function of the Reynolds number [43], Re, which for rectangular microchannels is defined as,

$$\mathrm{Re} = \frac{\rho U D}{\eta_0} = \frac{2\rho Q}{\eta_0 (w + h)} \tag{4}$$

where D is the hydraulic diameter and η_0 is the zero-shear fluid viscosity. The inertial effect is often deemed effective only when the cell (or more generally particle) Reynolds number, Re_c,

$$\mathrm{Re}_c = \mathrm{Re}\left(\frac{d}{D}\right)^2 \tag{5}$$

is in the order of one or more specifically ≥ 0.1 [43]. The relative contribution between the elastic and inertial lift forces can be characterized by the dimensionless elasticity number, El, i.e., the ratio of the Weissenberg number to Reynolds number,

$$El = \frac{Wi}{\mathrm{Re}} = \frac{\lambda \eta_0 (w+h)}{\rho w^2 h} \tag{6}$$

As the two lift forces scale differently with the (equivalent) spherical diameter, cells with dissimilar sizes and/or shapes can be potentially directed to distinct equilibrium positions in viscoelastic fluid flows through simple straight rectangular microchannels. This enables a continuous-flow, sheath-free, and high-efficiency separation, which has been demonstrated in previous studies for size-based separation of (approximately) spherical particles and cells [18, 30] as well as shape-based separation of equal-volumed particles [29].

3.2 Separation performance metrics

We evaluate the separation performance for both normal and multimeric yeast cells in terms of three dimensionless metrics [8]. The separation efficiency is defined as

$$efficiency = \frac{(N_i)_{zone}}{N_i} \tag{7}$$

where N_i is the total number of normal ($i = n$) or multimeric ($i = m$) cells at the channel outlet while $(N_i)_{zone}$ denotes the counted number of the same cell type within a specific zone of the channel outlet. The separation *purity* is defined as

$$purity = \frac{(N_i)_{zone}}{(N_n + N_m)_{zone}} \tag{8}$$

which measures the number of a target cell type (i.e., normal or multimeric) within a specific zone relative to that of all cells counted within the same zone at the channel outlet. The enrichment ratio, *ER*, is defined as the number ratio of one target cell type to the other within a specific zone at the channel outlet divided by the same ratio at the inlet. For example, the *ER* of normal cells is given by

$$ER = \frac{(N_n/N_m)_{zone}}{(N_n/N_m)_{inlet}} \tag{9}$$

4 Results and discussion

4.1 Demonstration of morphology-based yeast cell separation

Figure 3 shows the top-view images of the drug-treated yeast cells in the flow of PBS-based 1000 ppm PEO solution at the inlet (A) and the outlet expansion (B) of a 25 μm deep rectangular microchannel. The zoom-in views of the cells at these two locations are displayed as the inset plots I and II where the morphology of individual cells can be identified. The volumetric flow rate is 150 μL/h, and the calculated Reynolds and Weissenberg numbers are $Re = 0.48$ and $Wi = 9.47$, respectively. The corresponding cell Reynolds number is $Re_c = 0.02$ even for the larger multimeric cells with an average equivalent spherical diameter of 7 μm. Therefore, the inertial effect should be weak in this experiment and the elastic lift dominates the force exerted on the cells. At the channel inlet (Figure 3A), the normal and multimeric cells are both uniformed distributed and mixed. At the outlet expansion (Figure 3B), the smaller and more spherical normal cells appear to exit the channel inside a tight zone around the channel centerline, specifically within approximately one-third of the local channel half-width as highlighted in the inset plot II of Figure 3B. In contrast, the larger and less spherical multimeric cells are directed farther away from the centerline by the flow-induced lift force and found to exit the channel within the zone nearer to the sidewalls. This observation is consistent with our recent studies where both smaller spherical particles/cells [18, 30] and equal-volumed non-spherical particles [29] are elasto-inertially focused in 1000 ppm PEO solution toward symmetric equilibrium positions closer to the centerline (or more accurately, the center-plane) of straight rectangular microchannels. The quantitative analysis of the performance metrics for this sheathless elasto-inertial cell separation by morphology is presented in the following section on the study of flow rate effects.

4.2 Effect of flow rate

Figure 4 shows the influence of flow rate on the yeast cell separation in Figure 3 when all other conditions remain unvaried. With the increase of flow rate, the Reynolds and Weissenberg numbers both increase leading to enhanced inertial and elastic effects. The elasticity number, however, remains constant, and so the elastic lift should dominate in the entire range of flow rates. At 80 μL/h, all cells travel out of the straight microchannel in a single mixed stream about the centerline as viewed from the image in Figure 4A. However, the dispersion of the multimeric cells is apparently greater than that of the normal cells, which is illustrated in Figure 4B by the larger span of the former cells' exiting positions at the outlet expansion. At 100 μL/h, approximately half of the multimeric cells move away from the stream along the centerline (Figure 4A), and migrate toward a new equilibrium position that is about half way of the local half-width (Figure 4B). In

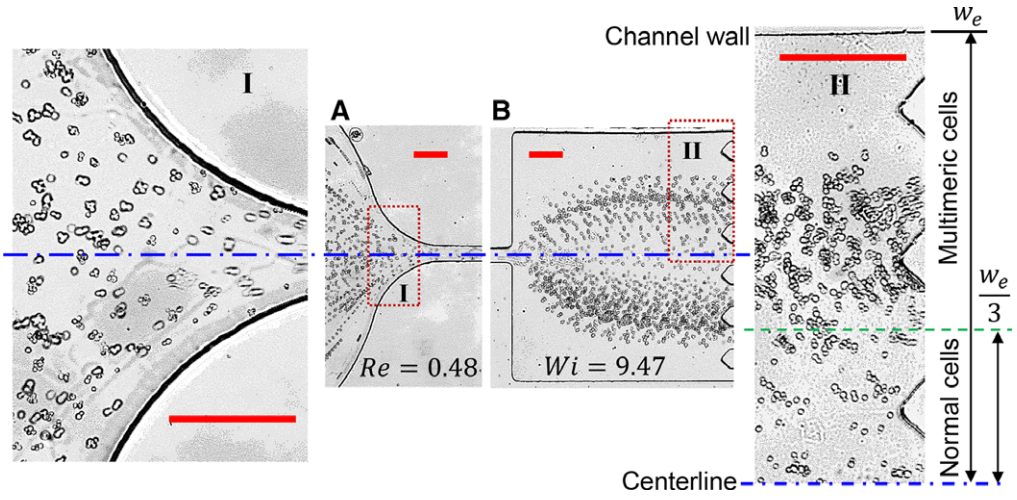

Figure 3. Top-view images of drug-treated *C. neoformans* cells in the flow of PBS-based 1000 ppm PEO solution at the inlet (A) and outlet expansion (B) of a 25 μm high straight rectangular microchannel. The inset plots I and II are the zoom-in views of the dashed-line highlighted regions at the channel inlet and outlet, respectively. The flow rate is 150 μL/h, and the corresponding values of the Reynolds number, *Re*, and Weissenberg number, *Wi*, are labeled on the images. The normal and multimeric cells are observed to exit the channel in the inner and outer zones of the outlet expansion that are divided at one-third of the local half-width, i.e., $w_e/3$, as indicated on inset II. The scale bars on all images represent 100 μm.

contrast, normal cells still stay near the centerline. When the flow rate is increased to 150 μL/h, the centerline equilibrium position disappears for both types of cells in Figure 4A. All the multimeric cells exit the channel at one-half of the local half-width while the normal cells have an average off-center exiting position of around one-quarter of the local half-width as seen from Figure 4B. Further increasing the flow rate shifts outward the equilibrium position of normal cells and hence reduces the gap from the equilibrium position of multimeric cells that remains fixed.

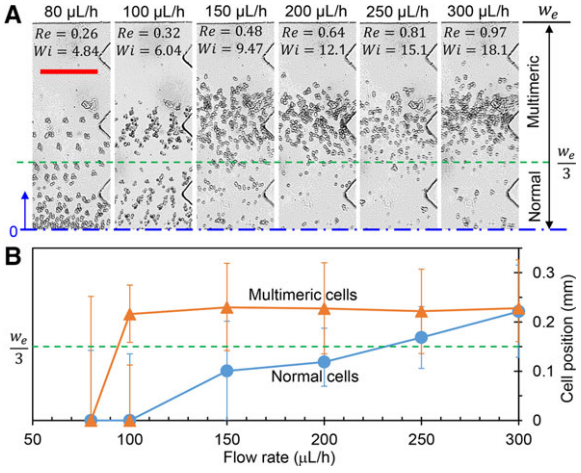

Figure 4. Flow rate effect on the elasto-inertial separation of drug-treated *C. neoformans* cells in the flow of PBS-based 1000 ppm PEO solution through a 25 μm deep rectangular microchannel: (A) the top-view images of cells in the upper-half of the outlet expansion; (B) the average exiting positions (symbols with error bars) of the normal and multimeric cells at the channel outlet (obtained from the images in (A) with respect to the channel centerline). The dashed line at the off-center position of one-third of the local channel half-width, i.e., $w_e/3$, in (A) and (B) divides the upper-half of the outlet expansion into the inner and outer zones for evaluating the separation performance metrics of normal and multimeric cells, respectively, in Figure 5. The calculated values of the Reynolds and Weissenberg numbers are labeled on the images in (A). The scale bar represents 100 μm.

Figure 5 plots the three performance metrics for the drug-treated yeast cell separation at different flow rates in Figure 4. They were evaluated using the definitions in Eqs. (7)–(9) for both the multimeric and the normal cells in the near-wall zone and the near-center zone, respectively. These outer and inner zones in the upper-half of the outlet expansion are split at the off-center position of one-third of the local channel half-width, i.e., the dashed line on the cell images in Figure 4A. The separation efficiency of multimeric cells increases from 30% at 80 μL/h to 93% at 150 μL/h and then stays roughly unchanged at higher flow rates (except 250 μL/h due to the significantly less number of cells counted in this test; see the image in Figure 4A). This is because the multimeric cells have all migrated into the outer zone at 150 μL/h and above. The separation purity of multimeric cells achieves the highest value of 94% at 100 μL/h and drops at higher flow rates because normal cells start appearing in the outer zone. In contrast, the separation efficiency and purity of normal cells reach the highest values, both over 90%, at 100 and 150 μL/h, respectively. As a result, the multimeric and normal cells each achieve a greater than 12 enrichment ratio at the flow rates of 100 and 150 μL/h, respectively. The best separation performance for both types of cells should take place in a flow rate in between.

4.3 Effect of polymer concentration

Figure 6 shows the influence of polymer concentration on the drug-treated yeast cell separation in PBS-based PEO solutions

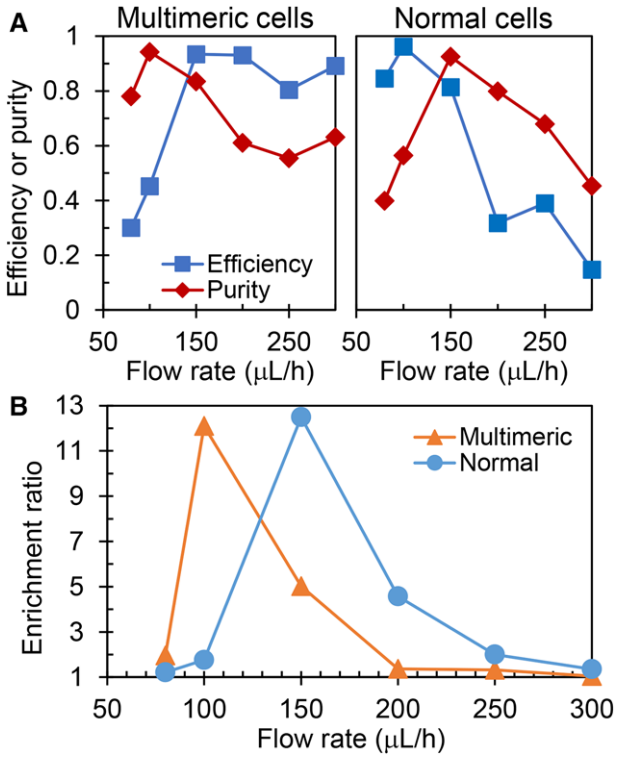

Figure 5. Performance metrics for the demonstrated elasto-inertial separation of drug-treated *C. neoformans* cells at different flow rates in 4 (A) the efficiency and purity for the multimeric (left plot) and normal (right plot) cells, respectively, and (B) the enrichment ratio of the two types of cells.

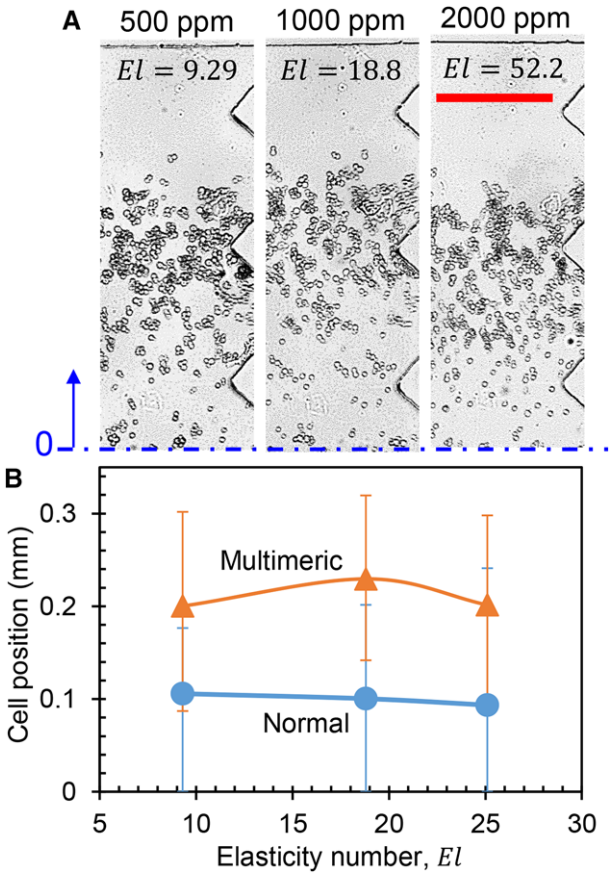

Figure 6. Polymer concentration effect on the elasto-inertial separation of drug-treated *C. neoformans* cells in the flow of PBS-based PEO solutions in a 25 μm deep microchannel: (A) the top-view images of cells in the upper-half of the outlet expansion; (B) the average exiting positions (symbols with error bars) of the multimeric and normal cells at the channel outlet (obtained from the images in (A) with respect to the channel centerline). The flow rate is fixed at 150 μL/h. The calculated values of the elasticity number are labeled on the images in (A). The scale bar in (A) represents 100 μm.

at a fixed flow rate of 150 μL/h. Increasing the PEO concentration increases the Weissenberg number (due to the longer fluid relaxation time) and decreases the Reynolds number (due to the larger fluid viscosity), leading to an increased elasticity number. Therefore, the elastic effect gets more dominant in a higher concentration PEO solution, which has been demonstrated in previous studies to shift the equilibrium positions of both spherical and non-spherical particles and cells [18, 29, 30]. This consequence is, however, not obviously viewed from the images of cells at the outlet expansion in Figure 6A due to perhaps the wide range of variations in both the size and shape of drug-treated yeast cells. Figure 6B compares the average exiting positions of the multimeric and normal cells at the outlet expansion, where the former is farther from the channel centerline in all three PEO concentrations. However, the focusing position of the larger and less spherical multimeric cells first shifts outward and then inward when the PEO concentration is increased from 500 to 1000 and 2000 ppm. In contrast, the focusing position of the smaller and more spherical normal cells slightly shifts inward with the increase of PEO concentration. Similar trends were also observed in our previous studies on spherical and peanut-shaped polystyrene particles [29, 30]. The best cell separation is achieved in ~1000 ppm PEO solution.

4.4 Effect of channel height

Figure 7 shows the influence of channel height on the drug-treated yeast cell separation in PBS-based 1000 ppm PEO solution. The channel width is fixed at 50 μm. In a 15 μm high channel, the multimeric and normal cells each possess two similar equilibrium positions as viewed from both the cell images at varying flow rates (Figure 7A, where only three flow rates are illustrated as examples) and the cell exiting positions at 150 μL/h (Figure 7B). The primary equilibrium position is about one-third of the local channel half-width away from the wall (as compared to the one-half in a 25 μm high channel; see Figure 4), and slightly shifts inward with the increase of flow rate. The secondary equilibrium position is along the channel centerline, which is also observed for polystyrene particles and other types of cells in previous studies [18,29,30]. In contrast, both types of yeast cells are directed toward the single equilibrium position along the channel centerline in

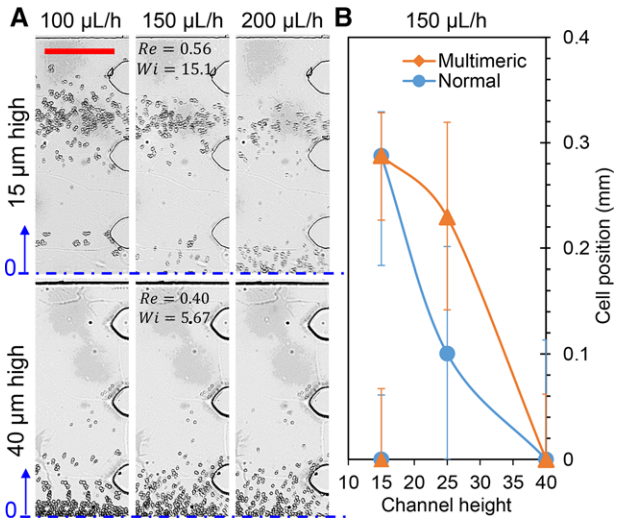

Figure 7. Channel height effect on the elasto-inertial separation of drug-treated *C. neoformans* cells in the flow of PBS-based 1000 ppm PEO solutions: (A) the top-view images of cells in the upper-half of the outlet expansion in 15 μm (top row) and 40 μm (bottom row) high microchannels at different flow rates; (B) the average exiting positions (symbols with error bars) of the multimeric and normal cells at the channel outlet (obtained from the images in (A) at the flow rate of 150 μL/h). The calculated values of the Reynolds and Weissenberg numbers at 150 μL/h are labeled on the images in (A). The scale bar in (A) represents 100 μm.

a 40 μm high channel when the flow rate is varying from 80 to 300 μL/h. Moreover, the elasto-inertial focusing gets improved at a higher flow rate for each type of cells (see the cell images in Figure 7A, where only three flow rates are illustrated). Therefore, the multimeric and normal cells cannot be effectively separated in a 15 μm or a 40 μm high channel. This result is consistent with our recent studies on polystyrene particle separation by shape [29] or size [30].

4.5 Concluding remarks

We have built upon our recent work [29, 30] to demonstrate a continuous-flow sheath-free separation of drug-treated *C. neoformans* cells by morphology in the flow of biocompatible PBS-based PEO solutions through straight rectangular microchannels. The heterogeneous mixture of yeast cells with varying shapes and sizes are elasto-inertially focused toward morphology-dependent equilibrium positions. Consistent with our previous observations for polystyrene particles [29, 30], the larger, abnormal-shaped multimeric cells are found to stay farther away from the channel center than the smaller, regular-shaped normal cells. We have studied the flow rate effect on this separation and evaluated its performance in terms of three dimensionless metrics including efficiency, purity, and enrichment ratio. We have also studied the effects of PEO concentration and channel height on the morphology-based yeast cell separation. The best separation performance is achieved in 1000 ppm PEO solution flow through an intermediate channel width/height ratio (two in the current work) at the flow rate of the order of 100 μL/h. It is noted that the molecular weight of PEO polymer can affect the elastic lift via the dependence of fluid shear thinning and elasticity [45]. We leave this parametric effect as a potential future study in order to further optimize the working conditions for cell separation. Moreover, we will collect the separated normal and multimeric cells for analysis of their drug resistance.

This work was supported in part by NIH under Grant 1R15 AI119801-01 (L.K.), and NSF under Grant CBET-1150670 (X.X.).

The authors have declared no conflict of interest.

5 References

[1] Casadevall, A., Perfect, J.R., *Cryptococcus neoformans*. American Society for Microbiology Press, Washington, DC 1998.

[2] Sionov, E., Lee, H., Chang, Y. C., Kwon-Chung, K. J., *PLoS Pathog.* 2010, *6*, e1000848.

[3] Altamirano, S., Fang, D., Simmons, C., Sridhar, S., Wu, P., Sanyal, K., Kozubowski, L., *mSphere* 2017, *2*, e00205–17.

[4] Sajeesh, P., Sen, A. K., *Microfluid. Nanofluid.* 2014, *17*, 1–52.

[5] Yan, S., Zhang, J., Yuan, D., Li, W., *Electrophoresis* 2017, *38*, 238–249.

[6] Karimi, A., Yazai, S., Ardekani, A. M., *Biomicrofluid.* 2013, *7*, 021501.

[7] Gossett, D. R., Weaver, W. M., Mach, A. J., Hur, S. C., Tse, H. T., Lee, W., Amini, H., Di Carlo, D., *Anal. Bioanal. Chem.* 2010, *397*, 3249–3267.

[8] Jadhao, V., Thomas, C. K., de la Cruz, M. O., *Proc. Natl. Acad. Sci. USA.* 2014, *111*, 12673–12678.

[9] Champion, J. A., Mitragotri, S., *Proc. Natl. Acad. Sci. USA.* 2006, *103*, 4930–4934.

[10] Martin, S. G., *Cell Cycle* 2009, *8*, 3643–3647.

[11] Hajba, L., Guttman, A., *Trends Anal. Chem.* 2017, *90*, 38–44.

[12] Sugaya, S., Yamada, M., Seki, M., *Biomicrofluid.* 2011, *5*, 24103.

[13] Yamada, M., Seki, M., *Lab Chip* 2005, *5*, 1233–1239.

[14] Beech, J. P., Holm, S. H., Adolfsson, K., Tegenfeldt, J. O., *Lab Chip* 2012, *12*, 1048–1051.

[15] Huang, L., Cox, E. C., Austin, R. H., Sturm, J. C., *Science* 2004, *304*, 987–990.

[16] Lu, X., Xuan, X., *Anal. Chem.* 2015, *87*, 11523–11530.

[17] Lu, X., Xuan, X., *Anal. Chem.* 2015, *87*, 6389–6396.

[18] Zhou, Y., Xuan, X., *Appl. Phys. Lett.* 2016, *109*, 102405.

[19] Chen, Q., Li, D., Zielinski, J., Kozubowski, L., Lin, J., Wang, M., Xuan, X., *Biomicrofluid.* 2017, *11*, 064102.

[20] Zhou, R., Bai, F., Wang, C., *Lab Chip* 2017, *17*, 401–406.

[21] Zhou, R., Sobecki, C. A., Zhang, J., Zhang, Y., Wang, C., *Phys. Rev. Appl.* 2017, *8*, 024019.

[22] Valero, A., Braschler, T., Rauch, A., Demierre, N., Barral, Y., Renaud, P., *Lab Chip* 2011, *11*, 1754–1760.

[23] Urdaneta, M., Smela, E., *Electrophoresis* 2007, *28*, 3145–3155.

[24] Kose, A. R., Fischer, B., Mao, L., Koser, H., *Proc. Natl. Acad. Sci. USA*. 2009, *106*, 21478–21483.

[25] DuBose, J., Lu, X., Patel, S., Qian, S., Joo, S. W., Xuan, X., *Biomicrofluid*. 2014, *8*, 014101.

[26] Zhu, J., Tzeng, T. J., Xuan, X., *Electrophoresis* 2010, *31*, 1382–1388.

[27] Masaeli, M., Sollier, E., Amini, H., Mao, W., Camacho, K., Doshi, N., Mitragotri, S., Alexeev, A., Di Carlo, D., *Phys. Rev. X* 2012, *2*, 031017.

[28] Li, M., Munoz, H. E., Goda, K., Di Carlo, D., *Sci. Rep.* 2017, *7*, 10802.

[29] Lu, X., Zhu, L., Hua, R., Xuan, X., *Appl. Phys. Lett.* 2015, *107*, 264102.

[30] Li, D., Lu, X., Xuan, X., *Anal. Chem.* 2016, *88*, 12303–12309.

[31] Perfect, J. R., Ketabchi, N., Cox, G. M., Ingram, C. W., Beiser, C. L., *J. Clin. Microbiol.* 1993, *31*, 3305–3309.

[32] Iwase, M., Okada, S., Oguchi, T., Toh-e, A., *Genes Genet. Syst*. 2004, *79*, 199–206.

[33] Liu, C., Xue, C., Chen, X., Shan, L., Tian, Y., Hu, G., *Anal. Chem.* 2015, *87*, 6041–6048.

[34] Yuan, D., Tan, S. H., Sluyter, R., Zhao, Q., Yan, S., Nguyen, N. T., Guo, J., Zhang, J., Li, W., *Anal. Chem.* 2017, *89*, 9574–9582.

[35] Tian, F., Zhang, W., Cai, L., Li, S., Hu, G., Cong, Y., Liu, C., Li, T., Sun, J., *Lab Chip* 2017, *17*, 3078–3085.

[36] Holzner, G., Stavrakis, S., deMello, A., *Anal. Chem.* 2017, *89*, 11653–11663.

[37] Bird, R. B., Armstrong, R. C., Hassager, O., *Dynamics of Polymeric Liquids, Vol.1*, Wiley, New York, NY 1977.

[38] D'Avino, G., Greco, F., Maffettone, P. L., *Annu. Rev. Fluid Mech.* 2017, *49*, 341–360.

[39] Xiang, N., Ni, Z., Yi, H., *Electrophoresis* 2018, *39*, 417–424.

[40] Del Giudice, F., Sathish, S., D'Avino, G., Shen, A. Q., *Anal. Chem.* 2017, *89*, 13146–13159.

[41] Lu, X., Liu, C., Hu, G., Xuan, X., *J. Colloid Interf. Sci.* 2017, *500*, 182–201.

[42] Di Carlo, D., *Lab Chip* 2009, *9*, 3038–3046.

[43] Di Carlo, D., Edd, J. F., Humphry, K. J., Stone, H. A., Toner, M., *Phys. Rev. Lett.* 2009, *102*, 094503.

[44] Asmolov, E. S., *J. Fluid Mech.* 1999, *381*, 63–87.

[45] Liu, C., Ding, B., Xue, C., Tian, Y., Hu, G., Sun, J., *Anal. Chem.* 2016, *88*, 12547–12553.

